water

MDPI

Article

Applications of Two-Dimensional Spatial Routing Procedure for Estimating Dispersion Coefficients in Open Channel Flows

Jaehyun Shin [1], Dongsop Rhee [1] and Inhwan Park [2,*]

[1] Korea Institute of Civil Engineering and Building Technology, 283, Goyangdae-Ro, Ilsanseo-Gu, Goyang-Si 10223, Gyeonggi-Do, Korea; jaehyunshin@kict.re.kr (J.S.); dsrhee@kict.re.kr (D.R.)
[2] Department of Civil Engineering, Seoul National University of Science and Technology, 232 Gongreung-Ro, Nowon-Gu, Seoul 01811, Korea
* Correspondence: ihpark@seoultech.ac.kr

Abstract: In this study, the performance of two routing procedures were evaluated to estimate the two-dimensional dispersion coefficients. The two-dimensional Stream-Tube Routing Procedure (2D ST-RP) has been widely used to obtain the dispersion coefficients from measured concentration-time curves under the frozen cloud assumption. Meanwhile, the Spatial Routing Procedure (2D S-RP) employs the spatial distributions of concentration to estimate the dispersion coefficients. The performance of the two routing methods were evaluated in aspect of the validity of the frozen cloud assumption and the applicability in the non-Fickian mixing. From the estimation results of dispersion coefficients, the results by the 2D ST-RP included errors due to skewed concentration-time curves which were created by violating the frozen cloud assumption. On the other hand, the 2D S-RP provides accurate dispersion coefficients in the same condition. The estimated results of dispersion coefficients in the meandering channel show that both the 2D ST-RP and the 2D S-RP contained errors due to the non-Fickian mixing properties of the test case. Even with the discrepancies, the 2D S-RP presented more appropriate spatial variabilities along the meander cycle than the results by the 2D ST-RP.

Keywords: dispersion coefficient; routing procedure; 2D ST-RP; 2D S-RP; frozen cloud assumption

check for updates

Citation: Shin, J.; Rhee, D.; Park, I. Applications of Two-Dimensional Spatial Routing Procedure for Estimating Dispersion Coefficients in Open Channel Flows. *Water* **2021**, *13*, 1394. https://doi.org/10.3390/w13101394

Academic Editors: Bommanna Krishnappan and Xiangyu Hu

Received: 1 April 2021
Accepted: 13 May 2021
Published: 17 May 2021

Publisher's Note: MDPI stays neutral with regard to jurisdictional claims in published maps and institutional affiliations.

Copyright: © 2021 by the authors. Licensee MDPI, Basel, Switzerland. This article is an open access article distributed under the terms and conditions of the Creative Commons Attribution (CC BY) license (https://creativecommons.org/licenses/by/4.0/).

1. Introduction

Pollutants in natural streams are transported by the temporal and spatial variations of shear flows. The shear flow dispersion is dominantly governed by the vertical deviations of longitudinal and transverse velocities from the depth-averaged velocity because the scale of shear flow is much larger than the turbulent fluctuations. These mixing phenomena in shear flow can be modeled using the two-dimensional (2D) advection-dispersion equation, which was derived from the depth-averaging process of three-dimensional advection diffusion [1]. The 2D advection-dispersion equation follows the Fick's law, which defines solute mass flux as the product of the concentration gradient and dispersion coefficient. The dispersion coefficient in the Fickian model has the important role of controlling not only the numerical dispersion but also the spatial dispersion of pollutants.

The calculation method of the dispersion coefficient can be classified into velocity-based and concentration-based methods. In the velocity-based method, dispersion coefficients are calculated using vertical profiles of longitudinal and transverse velocities [1]. Shen et al. [2] and Kim [3] calculated the longitudinal dispersion coefficients from the velocity measurements using an Acoustic Doppler Current Profiler (ADCP). Furthermore, Lee and Seo [4] analyzed the spatial properties of solute mixing in meandering channels from the calculation results of dispersion coefficients using velocity profiles. As the velocity-based method includes the effects of spatially varying velocity distributions, the method has advantages in reproducing shear dispersion processes using numerical models in meandering channels [5]. However, the velocity-based method tends to underestimate

dispersion coefficients compared to the concentration-based methods because the method neglects the effects of turbulent diffusion and storage zones [6,7]. Furthermore, it is difficult to obtain sufficient data from velocity structures because it requires significant time and costs. Thus, in natural streams, the bulk shear dispersion coefficients have been obtained from the concentration-based methods.

The concentration-based methods have been widely used to estimate the dispersion coefficients due to the aforementioned limitations of the velocity-based method. Previous tracer studies, which were conducted in laboratory channels [8,9] and natural streams [10,11], have been reported to evaluate shear dispersion in various flow conditions using temporal variations of concentration. From the concentration-time curves, dispersion coefficients have been estimated using the moment method or the routing procedure [12]. The moment method has been popularly used to obtain the transverse dispersion coefficient from the lateral variation of concentration-time curves [13–16]. However, the moment method is inappropriate to obtain the longitudinal dispersion coefficient for two-dimensional mixing problems. Thus, the two-dimensional stream-tube routing procedure was suggested to obtain the longitudinal and the transverse dispersion coefficients simultaneously [17]. These concentration-based methods were developed under the frozen cloud assumption, which considers time invariant shear dispersion while a tracer cloud is crossing a measuring cross-section [18]. The frozen cloud assumption is essential for estimating the dispersion coefficients using concentration-time curves measured at a fixed point; however, the estimated dispersion coefficients might include errors [19]. The limitations of the field observations, in which probes are installed at a fixed point to measure concentration-time curves, are being overcome by the research of image analysis that converts a tracer cloud taken from images by unmanned aerial vehicles into a concentration field [20–22]. It could be possible to obtain the dispersion coefficients without the frozen cloud assumption if spatial distributions of concentration are available to use.

In this study, performance of the two-dimensional Spatial Routing Procedure (2D S-RP) and the two-dimensional Stream-Tube Routing Procedure (2D ST-RP) was evaluated by comparisons of the estimated dispersion coefficients. As aforementioned, the 2D ST-RP employs the concentration-time curves under the assumption of frozen cloud. The 2D S-RP uses the spatial distributions of concentration to estimate the dispersion coefficients and the frozen cloud assumption is not required. From these two routing procedures, applicability was evaluated against two test cases: (1) idealized solute mixing problem; (2) 2D tracer test results conducted in a meandering channel. From the comparisons of estimated dispersion coefficients, the validity of the frozen cloud assumption was evaluated. In addition, the applicability of two routing procedures was discussed for tracer mixing showing non-Fickian mixing properties.

2. Material and Methods

2.1. Estimation of Dispersion Coefficients

2.1.1. Velocity-Based Method

Following the Fick's law, the solute transport in rivers was analyzed using the depth-averaged advection-dispersion equation under the assumption of large width to depth ratio. The depth-averaged advection-dispersion Equation is given as

$$\frac{\partial(hC)}{\partial t} + \frac{\partial(h\overline{u}_i C)}{\partial x_i} = \frac{\partial}{\partial x_i}\left(h\varepsilon_{ij}\frac{\partial C}{\partial x_j} - \int_0^h u'_j c'\, dz\right) \quad (1)$$

where C is the depth-averaged concentration; h is the water depth; t is the time; $\overline{u}_i$ is the depth-averaged velocity components in i-direction; ε_{ij} is the turbulent diffusion coefficient; $u'_j = u_j - \overline{u}_j$; u_j are the time-averaged velocity components in j-direction; $c' = c - C$; c is the concentration over flow depth. The second term in the right-hand side of Equation (1)

was defined by Fischer et al. [1], who extended the one-dimensional study of Taylor [23] to the 2D mixing problems as

$$-\frac{1}{h}\int_0^h u'_j c'\,dz = D_{ij}\frac{\partial C}{\partial x_j} \tag{2}$$

where D_{ij} is the dispersion coefficients in tensor form. Equation (2), which is called the Fickian dispersion model, has been widely used to simulate the 2D pollutant mixing [24–26]. The dispersion coefficients shown in Equation (2) can be calculated using the vertical profiles of velocity according to the theoretical derivation as

$$D_{ij} = -\frac{1}{h}\int_0^h u'_i \int_0^z \frac{1}{\varepsilon_v}\int_0^z u'_j\,dzdzdz \tag{3}$$

where ε_v is the vertical turbulent diffusion coefficient. In open channel flows, ε_v follows the parabolic distribution as

$$\varepsilon_v = \kappa h u^*\left(1-\frac{z}{h}\right) \tag{4}$$

where κ is the von Karman constant; $u^* = \sqrt{gR_hS_f}$ is the shear velocity; R_h is the hydraulic radius; S_f is the energy slope.

Dispersion coefficients in tensor form are efficient to simulate 2D solute mixing problems in the meandering channel [4]. However, Equation (3) is difficult to adopt in 2D models due to lack of vertical profiles of velocity. Thus, Alavian [27] suggested the coordinate transform method to define the dispersion coefficients into the tensor format. In the study by Alavian, dispersion tensor was derived using local velocity components in a fixed Cartesian coordinate and dispersion coefficients defined in the flow direction. Each component of a dispersion tensor is

$$D_{xx} = D_L\frac{\overline{u}^2}{\overline{u}^2+\overline{v}^2} + D_T\frac{\overline{v}^2}{\overline{u}^2+\overline{v}^2} \tag{5}$$

$$D_{xy} = D_{yx} = (D_L - D_T)\frac{\overline{u}\,\overline{v}}{\overline{u}^2+\overline{v}^2} \tag{6}$$

$$D_{yy} = D_T\frac{\overline{u}^2}{\overline{u}^2+\overline{v}^2} + D_L\frac{\overline{v}^2}{\overline{u}^2+\overline{v}^2} \tag{7}$$

where D_L and D_T are the longitudinal and transverse dispersion coefficients, respectively; $\overline{u}$ and $\overline{v}$ are the depth-averaged velocity component in x- and y-direction, respectively. When the flow direction coincides with x- or y-direction, dispersion by D_{xy} and D_{yx} is neglected and solute mixing is proceeded by D_{xx} and D_{yy}.

2.1.2. Concentration-Based Method

Routing Procedure Using Concentration-Time Curves

Methods for obtaining dispersion coefficients from the tracer test results can be classified into moment-based methods and routing procedures [17]. The moment-based methods have been used to estimate the transverse dispersion coefficient using continuous and transient tracer tests. The estimated dispersion coefficients using the moment method may include errors when the tracer clouds show the asymmetric distributions because values of the second moment do not provide proper relations following the Fick's law [28]. Furthermore, the moment method is not appropriate in obtaining the longitudinal dispersion coefficient. Thus, since the study by Fischer [29], several studies [17,30,31] have proposed routing procedures to compensate for the disadvantages of the moment method.

The routing procedure was first suggested by Fischer [29] for calculating the one-dimensional longitudinal dispersion coefficient. Following the study by Fischer, the routing procedure can be expanded to the two-dimensional case as follows [30]:

$$C(s_2,\ n,\ t) = \int_0^W \int_{-\infty}^{\infty} \frac{C(s_1,\ n',\ t')U}{4\pi(\bar{t}_2 - \bar{t}_1)\sqrt{D_L D_T}} \exp\left(-\frac{U^2(\bar{t}_2 - \bar{t}_1 - t + t')^2}{4D_L(\bar{t}_2 - \bar{t}_1)} - \frac{(n-n')^2}{4D_T(\bar{t}_2 - \bar{t}_1)} \right) dt'dn' \quad (8)$$

where $C(s_1,\ n,\ t)$ is the measured upstream concentration-time curves; $C(s_2,\ n,\ t)$ is the predicted downstream concentration-time curves; $\bar{t}_1$ and $\bar{t}_2$ are the average passage time of the tracer cloud; U is the cross-sectional average velocity. Using the two-dimensional routing procedure, the longitudinal and transverse dispersion coefficients can be obtained simultaneously using the upstream and downstream concentration-time curves. However, Equation (8) is inappropriate to use for a river that includes complex channel geometries.

Advancing from Equation (8), Baek and Seo [17] proposed the 2D ST-RP for adopting the routing procedure in irregularly varied channel width. The 2D ST-RP was derived by adopting the stream-tube concept as follows:

$$C(s_2,\ \eta,\ t) = \int_0^1 \frac{\left\{ \int_0^{\infty} \frac{C(s_1,\ n',\ \tau)U}{\sqrt{4\pi D_L(\bar{t}_2 - \bar{t}_1)}} \exp\left[-\frac{U^2(\bar{t}_2 - \bar{t}_1 - t + \tau)^2}{4D_L(\bar{t}_2 - \bar{t}_1)} \right] d\tau \right\}}{\sqrt{4\pi B_C(s_2 - s_1)}} \exp\left[-\frac{(\eta - n')^2}{4B_C(s_2 - s_1)} \right] dn' \quad (9)$$

where $B_C = \frac{\psi H^2 U}{Q^2} D_T$, ψ is the normalized shape factor defined as $\psi = \frac{1}{Q}\int_0^Q h^2 \overline{u}_s dq$; q is the cumulative discharge; η is the normalized cumulative discharge. From Equation (9), D_L and D_T can be obtained using the multiple regression algorithm. In this study, the non-linear regression algorithm of MATLAB software (Mathworks, Natick, USA), which finds the dispersion coefficients to predict best-fitted concentration curves, was adopted to estimate the dispersion coefficients.

Routing Procedure Using Spatial Distributions of Concentration

Usually, tracer tests have been conducted by measuring concentrations of tracer material at a fixed point, and the measured data provide the temporal variations of concentration. Therefore, the routing procedure using the concentration-time data requires the frozen cloud assumption in which the concentration curve does not experience change of dispersion during passage through the fixed sensors. However, the routing method under the frozen cloud assumption needs to be validated to determine whether the assumption causes errors to the estimated dispersion coefficients. Thus, in this study, the routing procedure using the spatial concentration distributions was adopted for estimating the dispersion coefficients. In the case of using the routing method using the spatial concentration distributions measured at a specific moment, it is possible to calculate the dispersion coefficients without incorporating the frozen cloud assumption.

From the analytic solution of the two-dimensional advection-dispersion equation, the two-dimensional spatial routing procedure (2D S-RP) can be derived as follows:

$$C(s,\ n,\ t_2) = \int_0^W \int_{-\infty}^{\infty} \frac{C(s',\ n',\ t_1)}{4\pi\Delta t\sqrt{D_L D_T}} \exp\left[-\frac{(s - s' - \overline{u}_s\Delta t)^2}{4D_L\Delta t} - \frac{(n - n' - \overline{u}_n\Delta t)^2}{4D_T\Delta t} \right] ds'dn' \quad (10)$$

where $C(s,\ n,\ t_1)$ is the upstream concentration field; $C(s,\ n,\ t_2)$ is the predicted downstream concentration field. D_L and D_T in Equation (10) were estimated as the non-linear regression algorithm, which is the same algorithm used for obtaining the dispersion coefficients using the 2D ST-RP method. Figure 1 shows the conceptual diagram of the two routing procedures, which are the 2D ST-RP and the 2D S-RP. The main difficulty of the 2D S-RP is that it is difficult to obtain the spatial concentration distributions in a field study. Therefore, in this study, 2D simulation results using the PDM-2D were employed for application of the 2D S-RP.

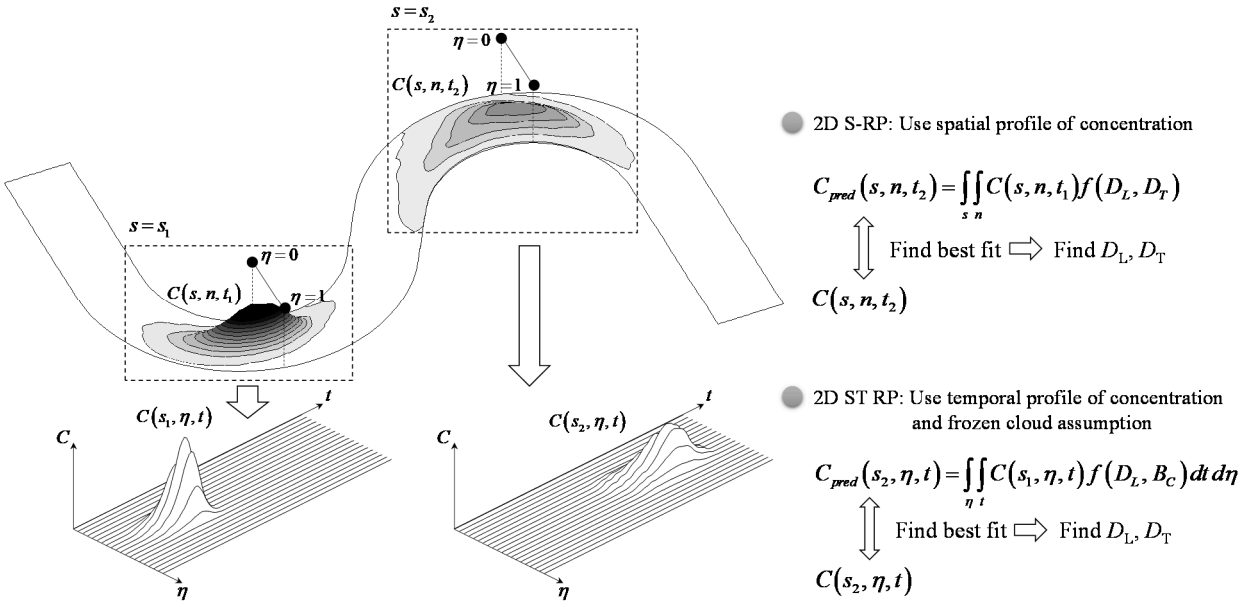

Figure 1. Conceptual diagram of routing procedures using spatial and temporal concentration measurements.

2.2. Model Descriptions

Park and Seo [32] developed the 2D Particle Dispersion Model (PDM-2D) to simulate two-dimensional pollutant mixing in rivers without input of dispersion coefficients based on the study by Fischer [29]. In the study by Fischer, the solute mixing was analyzed using step-by-step computations according to the physical interpretations of the shear dispersion instead of solving the advection-dispersion equation using numerical schemes. The PDM-2D calculates the 2D pollutant mixing using the two sequential calculation steps: (1) horizontal translation and (2) vertical mixing. Figure 2 describes the aforementioned computation procedures of the PDM-2D.

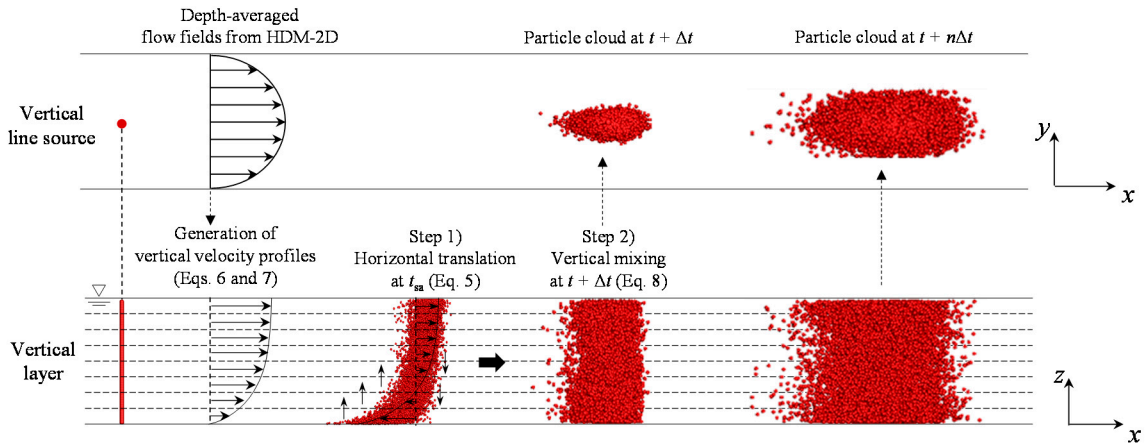

Figure 2. Computation procedures of the PDM-2D.

As described in Figure 2, in the horizontal translation step of PDM-2D, the individual particle position was calculated as follows:

$$\tilde{x}_i^k(z,\ t_{sa}) = x_i^k(z,\ t) + u_i\left(x_i^k,\ z,\ t\right)\Delta t + R\sqrt{2\varepsilon_h \Delta t} \tag{11}$$

where x_i^k is the k^{th} particle position in i-direction; $\tilde{x}_i^k$ is the particle position after shear advection; t_{sa} is the time after shear advection; z is the vertical position of each particle; Δt is the time step; R is the random number following the Gaussian distribution; ε_h is the

horizontal turbulent diffusion coefficient in the assumption of isotropic turbulence. The second term of the right-hand side in Equation (11) indicates the deterministic transport by vertically varied velocity profiles, and the third term is the transport of random fluctuations by the turbulent diffusion. The solute column is stretched on the horizontal planes by the vertical profiles of longitudinal (u_s) and transverse velocities (u_n), as shown in Figure 2. The vertical velocity profiles were generated using theoretical and empirical formulas, which can be reproduced using the depth-averaged flow fields. In the longitudinal direction, the log-profile suggested by Rozovskii [33] was employed to generate the vertical profile as

$$u_s(z) = \overline{u}_s\left[1 + \frac{\sqrt{g}}{\kappa C_h}\left(1 + \ln\frac{z}{h}\right)\right] \tag{12}$$

where C_h is the Chezy coefficient. The log-profile was granted with several experimental and theoretical supports as the longitudinal velocity profile [34]. For the shear flow of transverse direction, the secondary flow of the first kind needs to be reproduced in meandering channels. Thus, the linear profile reported by Odgaard [35] was adopted to generate the secondary currents as follows:

$$u_n(z) = \overline{u}_n + 2v_s\left(\frac{z}{h} - \frac{1}{2}\right)\left(v_s = \overline{u}_s\frac{h}{r_c}\left(\frac{2\kappa C_h + \sqrt{g}}{2\kappa^3 C_h}\right)\right) \tag{13}$$

The linear profile shown in Equation (13) was developed under the assumptions of steady, subcritical and isotropic turbulence, and the profile is applicable in channels with constant channel width and large r_c. The depth-averaged flow fields ($\overline{u}_s$, $\overline{u}_n$) for generating the vertical velocity profiles were computed using the depth-averaged hydrodynamic model, which is the Hydro Dynamic Model-2D (HDM-2D) using the shallow water equations [36]. The HDM-2D has been verified for several study cases, and the results were compared with the theoretical and experimental studies [37–39].

In the vertical mixing step, transported particles on each horizontal plane migrate on the upper or lower plane to complete the 2D mixing. The PDM-2D calculates the vertical position of particles using the vertical mixing scheme, suggested under the assumption of negligible small vertical velocity in natural streams as

$$\begin{cases} x_i^k(z,\ t+\Delta t) = \widetilde{x}_i^k\left(\alpha\frac{h}{L},\ t_{sa}\right) & \text{for full} - \text{column mixing} \\ x_i^k(z,\ t+\Delta t) = \widetilde{x}_i^k\left(z + R\sqrt{2\varepsilon_v\Delta t},\ t_{sa}\right) & \text{for random mixing} \end{cases} \tag{14}$$

where L is the number of horizontal layers; α is an arbitrary integer from 1 to L. In each computation step, a fraction of particles was evenly distributed by the full column mixing scheme, and remaining particles were randomly transported by the random mixing scheme. Through these two sequential computations, a step of shear dispersion is completed, and computations of pollutant mixing can be conducted without input of the dispersion coefficients [32]. The particle distributions can be converted to concentration fields for further analysis as

$$C(x_i,\ t) = \frac{mn(x_i,\ t)}{h\Delta A} \tag{15}$$

where m is mass of a single particle; $n(x_i,\ t)$ is the number of particles within water column; ΔA is the unit area includes $n(x_i,\ t)$ particles.

2.3. Generation of Concentration Fields for Estimating Routing Procedures

2.3.1. Idealized Concentration Fields to Evaluate the Frozen Cloud Assumption

For validation of the frozen cloud assumption, the dispersion coefficients for an idealized solute mixing problem were estimated using both the 2D ST-RP and the 2D S-RP. The test was conducted in the straight channel of the rectangular cross-section with 2 m

width. Under the unsteady flow condition, instantaneously injected solute mixing can be calculated using the analytic solution as

$$C(x,\ y,\ t) = \frac{M}{4\pi t\sqrt{D_L D_T}} \exp\left[-\frac{(x - x_0 - \overline{u}_s(t)t)^2}{4D_L t} - \frac{(y - y_0)^2}{4D_T t}\right] \tag{16}$$

$$\overline{u}_s(t) = 0.25 \sin t + 0.7 \tag{17}$$

where $(x_0,\ y_0)$ is the injection point of the solute; M is the inputted mass. The unsteady flow condition shown in Equation (17) was considered to evaluate the routing procedures, while the frozen cloud assumption was not maintained. In Equation (16), the longitudinal dispersion coefficient was assumed as $D_L = 5.93hu^* = 0.163\ \mathrm{m}^2/\mathrm{s}$, adopted from the study by Elder [40]. In the case of the transverse dispersion coefficient, $D_T = 0.15hu^* = 0.0041\ \mathrm{m}^2/\mathrm{s}$ was employed which was suggested for a straight channel [41]. The spatial distribution of concentration reproduced using Equation (16) was plotted in Figure 3, in which the concentration fields show the symmetric distributions following the Fickian dispersion. The cross-section for application of the 2D ST-RP shown in Figure 3 was determined, where the peak concentration is located where the solute clouds were drawn. By assuming that nineteen sensors are installed along uniform intervals across each cross-section, the concentration time curves were extracted to observe the temporal variations of concentration under the unsteady flow condition. The concentration-time curves at the center of each cross-section were plotted in Figure 4. According to the unsteady flow condition, the concentration curves show skewed distributions, which indicate the mixing is not stably maintained while a solute cloud passes through a cross-section. From these theoretical concentration data, performance of the 2D S-RP and the 2D ST-RP was evaluated against these solute mixing problems that violate the frozen cloud assumption.

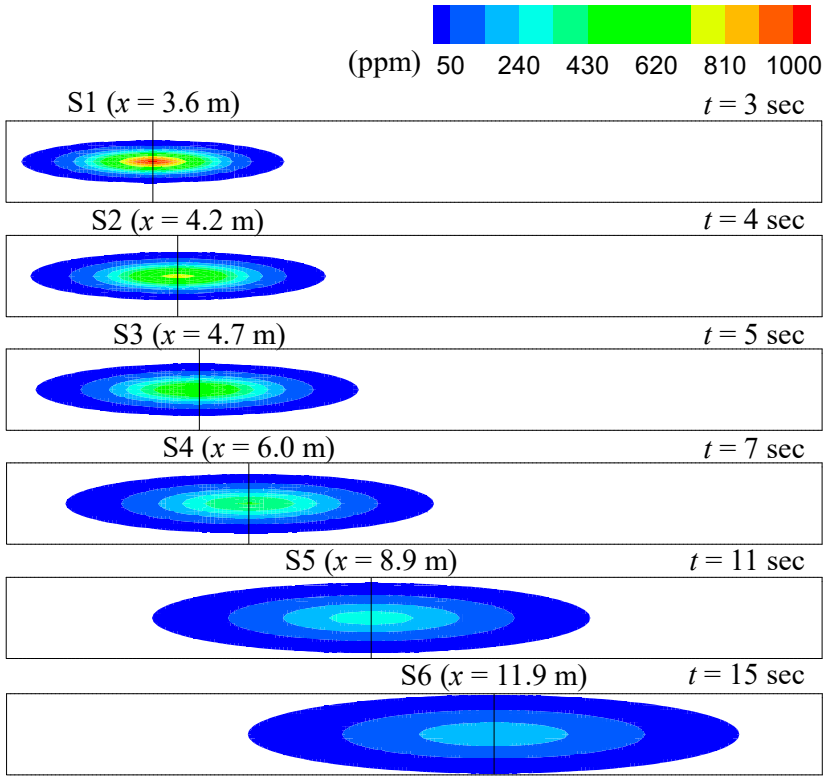

Figure 3. Concentration fields for estimating the dispersion coefficients using the 2D S-RP.

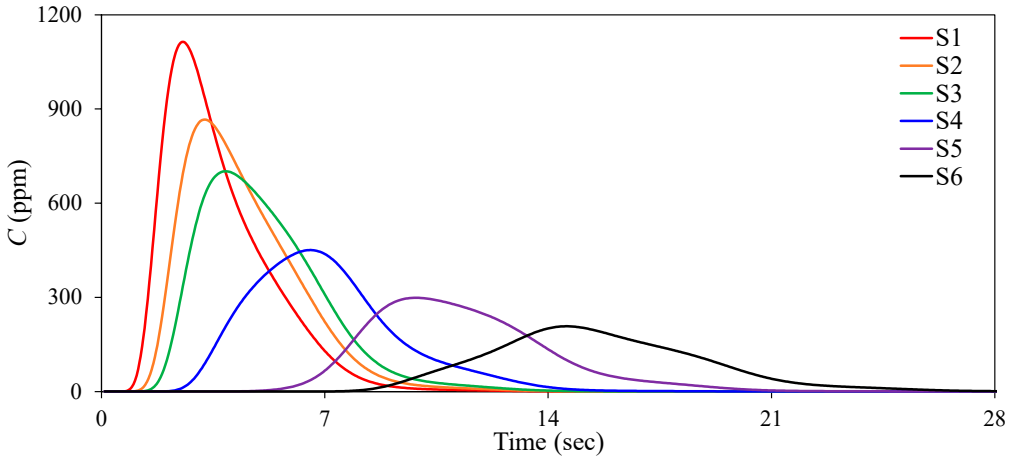

Figure 4. Concentration-time curves at the center of the cross-section for testing the 2D ST-RP.

2.3.2. Generation of Concentration Fields in M2 Channel Using the PDM-2D Simulation Results

Two routing procedures were applied to estimate dispersion coefficients of the two-dimensional tracer test results conducted in the laboratory meandering channel (M2 channel) by Seo and Park [9]. The tracer test was conducted using 100,000 ppm (C_0) of the brine and ethanol mixture as a tracer material. The outline of M2 channel was depicted in Figure 5 where the channel has rectangular cross-sections with 1 m width and two curved parts, and the experimental conditions were listed in Table 1. The tracer material was instantaneously introduced at 0.5 m upstream from the first measurement section (S1), and the concentration-time curves were measured using six conductivity sensors installed across each channel cross-section. The 2D ST-RP can be applied using the measured concentration-time curves. However, in the case of the 2D S-RP, spatial distributions of concentration are required, and the data can be obtained from aerial photos of tracer cloud or simulation results. In this study, the concentration fields were obtained from the simulation results by the PDM-2D, which has been validated by comparing to the tracer studies [32].

Following the experimental conditions shown in Table 1, the depth-averaged velocity distribution in the M2 channel was computed using the HDM-2D, as shown in Figure 5a. Based on the HDM-2D simulation results, the particle tracking simulations were conducted using the PDM-2D, and the particle distributions (Figure 5b) were converted to the concentration fields using Equation (15) (Figure 5c). For the simulation results, independence of the time step was checked for Δt = 0.125, 0.25, and 0.5 s, as shown in Figure 6. There was a difference according to the randomness of the particle motion, but the overall shape of concentration-time curves presented similar. As Δt decreased from 0.5 s to 0.25 and 0.125 s, the R-squared value of the simulation results showed 0.91, 0.88, and 0.89 in S6, and also 0.99, 0.98, and 0.96 in S9, respectively. Thus, 0.5 s of time step was used for this study, as listed in Table 1.

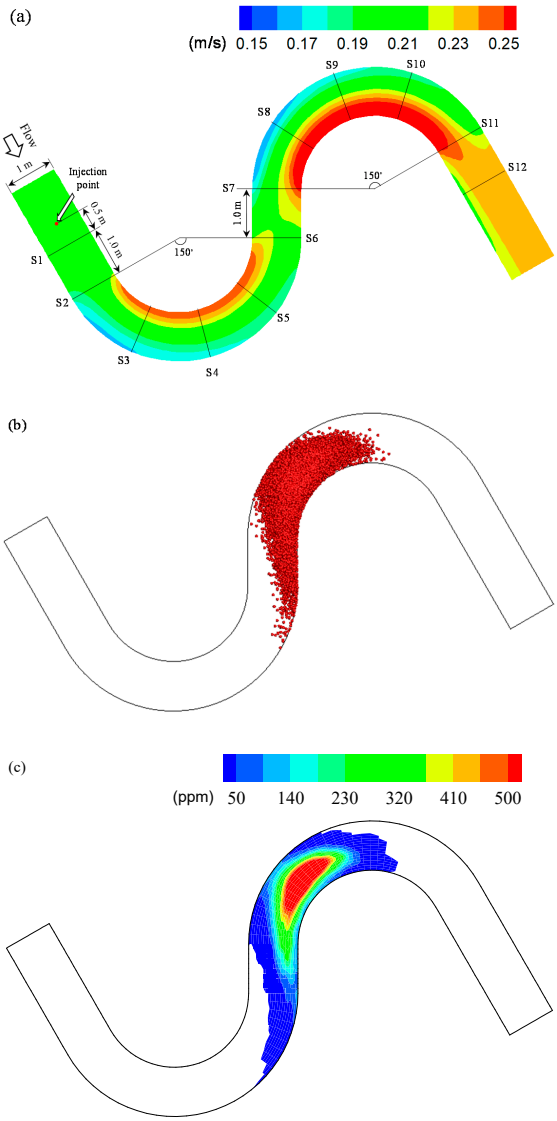

Figure 5. Outlines of M2 channel and the solute transport simulation results by the PDM-2D: (**a**) velocity contour; (**b**) particle distribution; (**c**) concentration distribution.

Table 1. Experimental results and simulation conditions for solute mixing in the M2 channel.

Q (m^3/s)	h (m)	U (m/s)	u^* (m/s)	C_0 (ppm)	Δt (s)	L	No. of Particles
0.06	0.4	0.15	0.0078	100,000	0.5	300	30,000

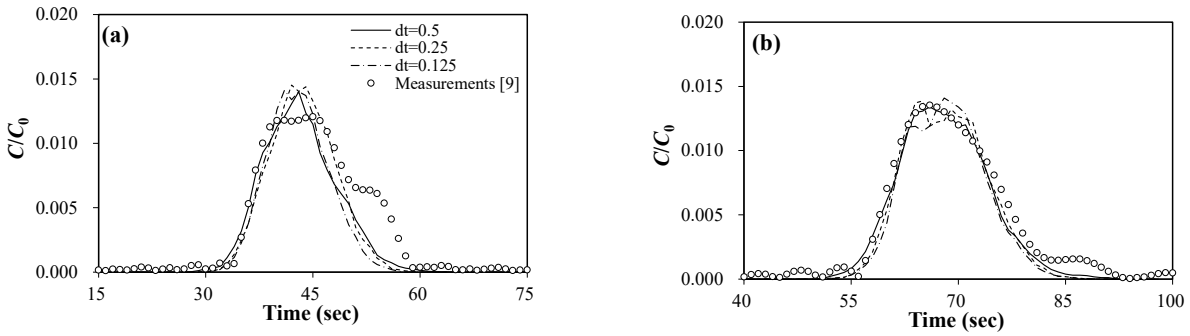

Figure 6. Comparisons of concentration-time curves at $y/W = 0.5$ for checking the time step dependence: (**a**) S6; (**b**) S9.

The concentration-time curves were plotted and compared with the simulation results in Figure 7. From the comparisons, the shape of concentration curves adequately reproduced the results of tracer mixing in the M2 channel. The statistical properties of concentration curves were listed in Table 2, in which the dimensionless peak concentration (C_p/C_0), the time to C_p (t_p), centroid (μ_t) and the skewness coefficient (ξ_t) were compared to the measurements. From the comparisons, discrepancies of the statistical values prominently appeared at $y/W = 0.70$ of S5 and S6. Even though the results include local errors, the statistical values indicate that the values of ξ_t were quite similar to the measurements of S6 and S9, which mean the shape of concentration curves were reasonable to represent the tracer mixing. Thus, the simulation results by the PDM-2D adequately reproduced pollutant mixing without input of the dispersion coefficients, and the simulation results were adopted to apply the 2D S-RP.

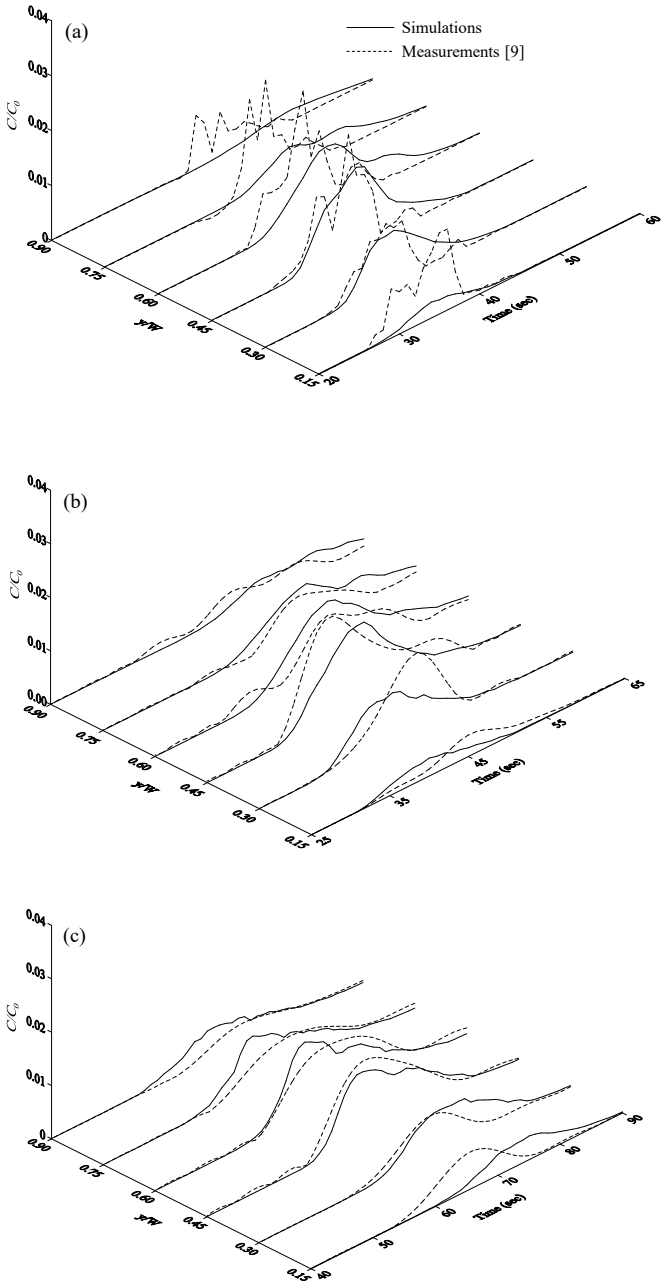

Figure 7. Comparisons of concentration-time curves in the M2 channel: (**a**) S5; (**b**) S6; (**c**) S9.

Table 2. Comparisons of statistical properties of concentration-time curves in the M2 channel.

Section No.	y/W	C_p/C_0		t_p (s)		μ_t (s)		ξ_t	
		Exp.	Sim.	Exp.	Sim.	Exp.	Sim.	Exp.	Sim.
S5	0.30	0.013	0.011	35.3	36.0	34.9	36.1	0.72	0.63
	0.45	0.022	0.021	37.1	38.0	36.6	38.3	0.43	0.59
	0.70	0.030	0.006	39.8	41.0	40.5	43.8	0.92	0.36
S6	0.30	0.014	0.009	44.8	42.0	44.4	42.5	0.29	0.62
	0.45	0.020	0.015	40.5	45.0	43.9	45.3	0.60	0.68
	0.70	0.008	0.011	50.1	51.0	50.7	52.1	0.16	0.54
S9	0.30	0.008	0.008	67.5	0.44	68.1	71.6	0.44	0.41
	0.45	0.015	0.013	65.3	0.56	68.2	69.3	0.56	0.62
	0.70	0.008	0.013	69.3	0.62	72.0	68.5	0.62	0.58

3. Results

3.1. Evaluations of the Frozen Cloud Assumption

The frozen cloud assumption, which is a fundamental theory of the routing procedures using temporal concentration data, was evaluated from the idealized solute mixing problem defined in Section 2.3.1. From the concentration data shown in Figures 3 and 4, longitudinal and transverse dispersion coefficients were estimated using both the 2D ST-RP and the 2D S-RP. Figure 8 shows the comparison results between the predicted concentration fields using the 2D S-RP and the analytic solution by Equation (16). The results shown in Figure 8 were predicted from the concentration field at t = 3 s as the upstream concentration data. The results show that the predicted concentration fields tend to underestimate the high concentration area, but the entire shape of the solute cloud was adequately estimated. The R-squared values of the predicted results denoted in Figure 8 indicate that the 2D S-RP appropriately estimated the downstream concentration fields.

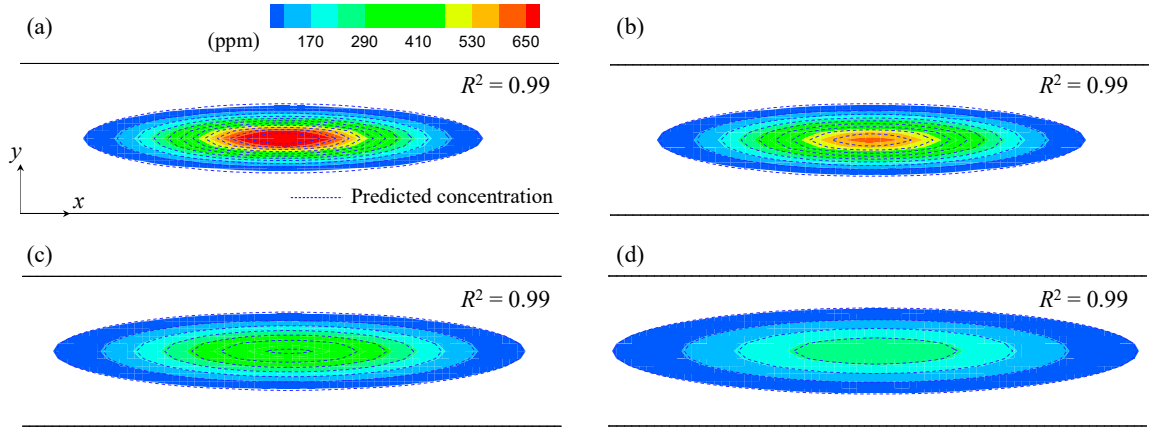

Figure 8. Comparisons of the analytic solution and the predicted concentration fields by the 2D S-RP: (**a**) t = 4 s; (**b**) t = 5 s; (**c**) t = 7 s; (**d**) t = 11 s.

Figure 9 shows contours of the concentration-time curves which were calculated using the 2D ST-RP. The predictions were performed using the concentration-time data of the section S1 shown in Figure 4 as the upstream concentration data. The contour plots of *C-t-y* curves show asymmetric distributions by the unsteady velocity conditions. Even if the R-squared values showed quite accurate results, the predicted concentration curves have discrepancies in the low concentration part where the concentration curves create long tails, as shown in Figure 4. From these results, it can be said that the 2D S-RP is more appropriate to estimate the concentration fields than the 2D ST-RP for a mixing problem where the frozen cloud assumption is not required.

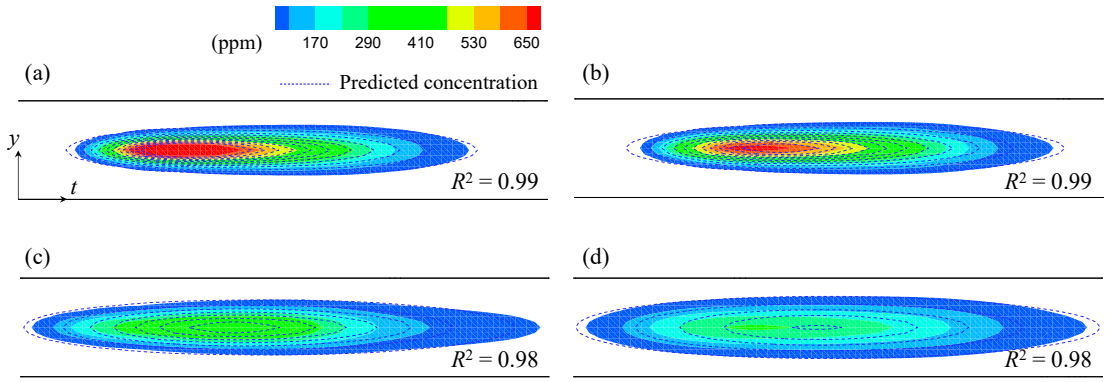

Figure 9. Comparisons of the analytic solution and the concentration-time contours by the 2D ST-RP: (**a**) S2; (**b**) S3; (**c**) S4; (**d**) S5.

The longitudinal and transverse dispersion coefficients inputted in Equation (16) were estimated using both the 2D S-RP and the 2D ST-RP. Table 3 shows the calculation results of the dispersion coefficients. The 2D S-RP provides stable results whether the routing span is changed, and the estimated D_L and D_T were exactly same to the inputted value. However, the results by the 2D ST-RP differed according to the selection of the routing span, and the results contained errors in the range of 1.2–43.7% for D_L and 1.8–40.6% for D_T. These errors were caused by discrepancies of the predicted concentration to the asymmetric concentration curves, which were created due to the unsteady flow condition because the routing procedure was developed based on the Fick's law following the Gaussian distribution.

Table 3. Calculation results of the dispersion coefficients using the 2D S-RP and the 2D ST-RP in the test conditions.

Routing Span	D_L (m^2/s)			D_T (m^2/s)		
	2D ST-RP	**2D S-RP**	**Analytic Solution**	**2D ST-RP**	**2D S-RP**	**Analytic Solution**
S1-S2	0.135	0.163	0.163	0.0048	0.0041	0.0041
S1-S3	0.166	0.163		0.0047	0.0041	
S1-S4	0.178	0.163		0.0051	0.0041	
S1-S5	0.136	0.163		0.0033	0.0041	
S1-S6	0.165	0.163		0.0027	0.0041	
Avg.	0.156	0.163		0.0041	0.0041	
S2-S3	0.153	0.163		0.0042	0.0041	
S2-S4	0.196	0.163		0.0057	0.0041	
S2-S5	0.141	0.163		0.0050	0.0041	
S2-S6	0.173	0.163		0.0051	0.0041	
Avg.	0.166	0.163		0.0050	0.0041	
S3-S4	0.195	0.163		0.0058	0.0041	
S3-S5	0.134	0.163		0.0050	0.0041	
S3-S6	0.170	0.163		0.0050	0.0041	
Avg.	0.166	0.163		0.0053	0.0041	
S4-S5	0.144	0.163		0.0038	0.163	
S4-S6	0.092	0.163		0.0042	0.0041	
Avg.	0.118	0.163		0.0040	0.0041	
S5-S6	0.208	0.163		0.0044	0.0041	

3.2. Estimations of the Dispersion Coefficients in Meandering Channel

The applicability of the 2D ST-RP and the 2D S-RP were compared by estimating dispersion coefficients of the M2 channel described in Section 2.3.2. The 2D S-RP used the simulation results shown in Figure 5 due to absent measured spatial distributions of

concentration. For application of the 2D S-RP, two concentration fields located upstream and downstream against each cross-section were selected from the simulation results. The best-fitted downstream concentration fields could be obtained when the optimal dispersion coefficients were found. Figure 10 shows the comparisons of the predicted and downstream concentration fields. The predicted concentration field adequately reproduced the spatial distribution of concentration, but inconsistency occurred in the high concentration area. The R-squared values for the comparison results were in the range of 0.98–0.99. The results by the 2D ST-RP are presented in Figure 11, in which the concentration curves were plotted in space-time domain. From the comparisons, the predicted concentration-time curves showed relatively inaccurate results, with a 0.85–0.86 range of R-squared values.

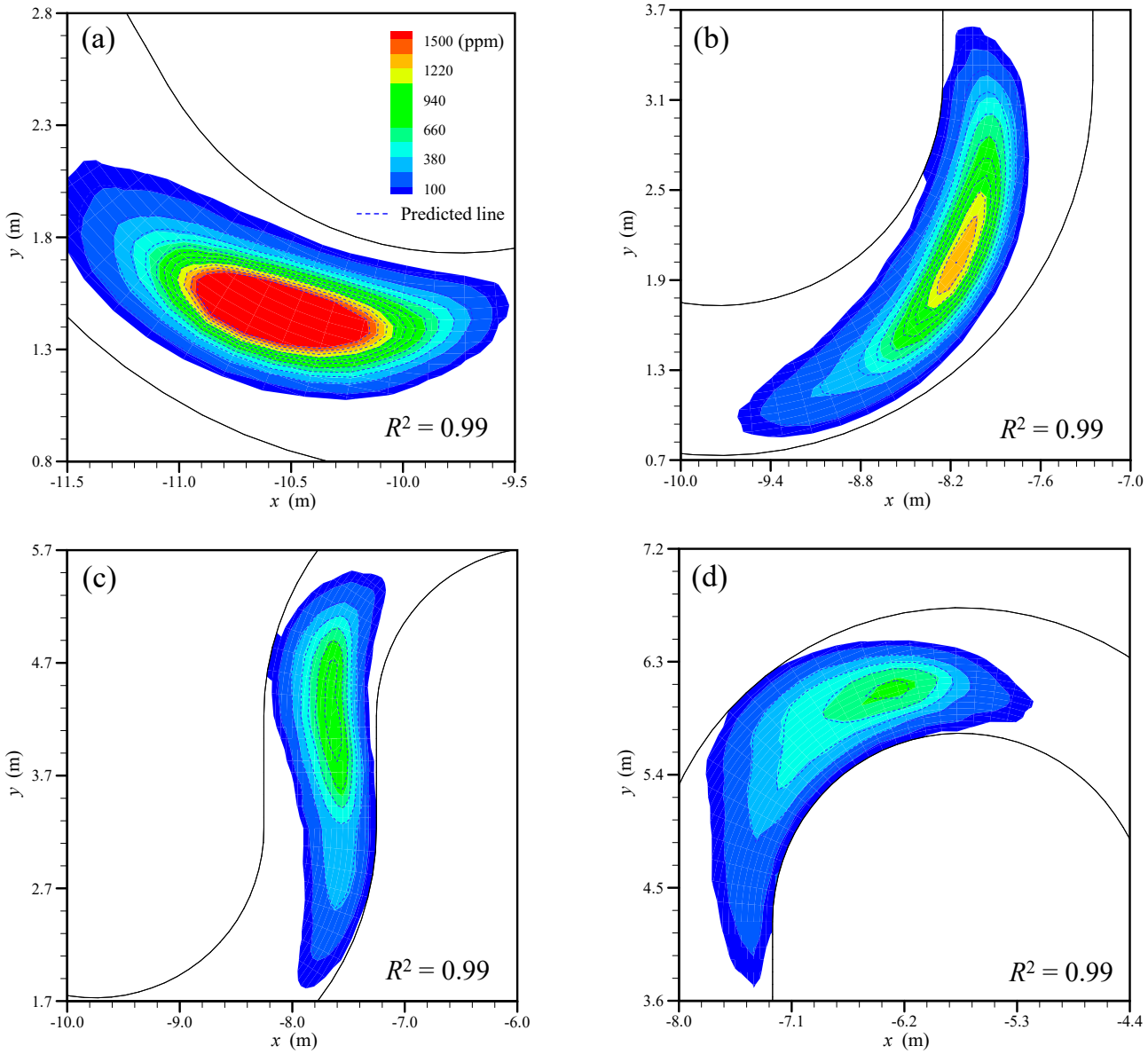

Figure 10. Comparisons of predicted concentration fields using the 2D S-RP: (**a**) S3; (**b**) S5; (**c**) S7; (**d**) S9.

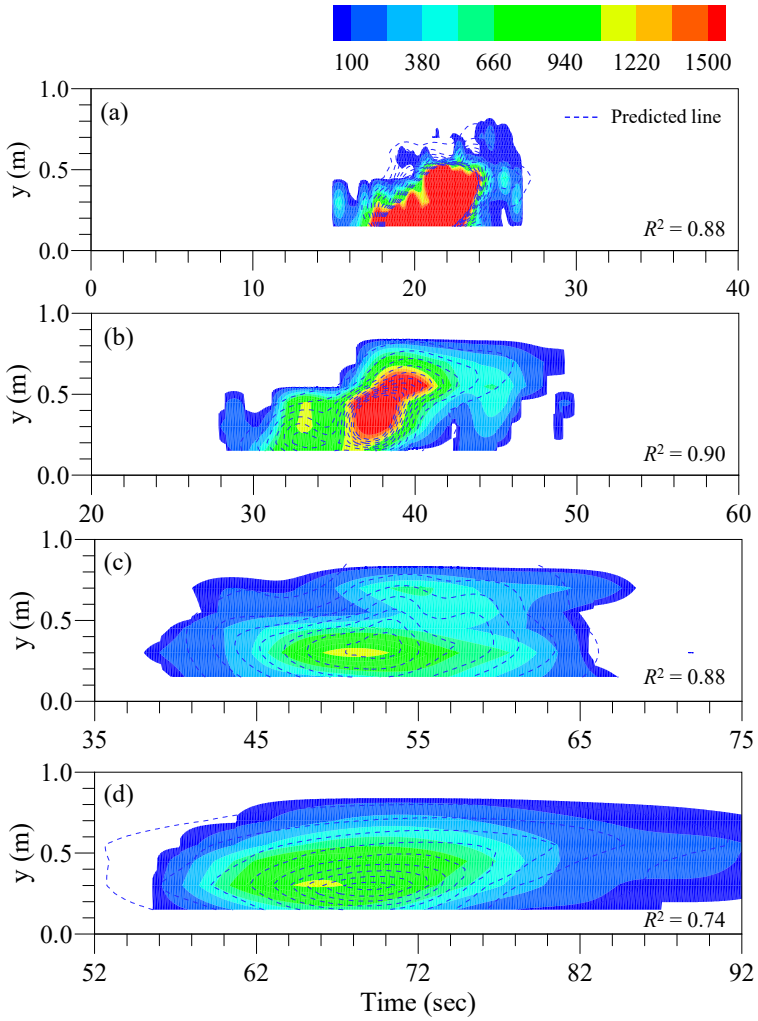

Figure 11. Comparisons of predicted concentration-time distributions using the 2D ST-RP: (**a**) S3; (**b**) S5; (**c**) S7; (**d**) S9.

The dispersion coefficients obtained using the 2D S-RP were compared with the results using the 2D ST-RP. Table 4 shows the comparisons of the dimensionless dispersion coefficients in each cross-section. Both results show that the longitudinal and the transverse dispersion increase in the cross-over (S6 and S7) and the curved (S4 and S8) parts of the channel, respectively. The overall variability of the dispersion coefficients along the entire channel were found to be greater for the 2D ST-RP than the 2D S-RP.

Table 4. Comparisons of dimensionless dispersion coefficients using the 2D ST-RP and the 2D S-RP.

Section No.	D_L/hu^*		D_T/hu^*	
	2D ST-RP	2D S-RP	2D ST-RP	2D S-RP
2	0.89	3.33	2.19	0.22
3	0.08	1.49	0.11	0.31
4	0.09	1.37	1.09	0.52
5	1.81	1.14	0.27	0.56
6	5.95	2.52	0.09	0.43
7	4.73	2.64	0.27	0.47
8	1.38	2.44	0.34	0.46
9	3.80	2.73	0.02	0.39
10	4.33	2.85	0.11	0.38

In natural streams, the dispersion coefficient includes shear flow and storage effects due to channel irregularities [7]. However, the results shown in Table 4 can be considered to only include the effect of shear flows because the M2 channel has uniform channel width and flow depth. Thus, the results using both routing procedures could be compared with the dispersion tensors of Equation (3), which explain the shear dispersion due to the velocity structures. For the calculations, the vertical profiles of x- and y-direction velocities measured by Seo and Park [9] were employed. To convert the dispersion coefficients shown in Table 4 to the tensor format, the coordinate transform method shown in Equations (5)–(7) was used.

The comparisons of the dispersion tensors were plotted in Figure 12, in which the dispersion tensors by Equation (3) were denoted as DF. The DF shows periodic patterns in which D_{xx}/hu^* increases in the bends of the channel and decreases in the cross-over part, whereas D_{yy}/hu^* shows an opposite pattern of decreasing in the bends and increasing in the cross-over part. The 2D S-RP provides the similar periodic patterns to the DF even though D_{xx}/hu^* in the first bend was underestimated compared to the DF. The local errors were deduced to occur due to the discrepancies of the simulation results, which were necessary for application to the 2D S-RP, because the predicted concentration fields shown in Figure 12 provided acceptable results. In case of the dispersion coefficients in the 2D ST-RP, D_{xx}/hu^* successfully reproduced dispersion in downstream of the section S6. However, other components of the dispersion tensor show discrepancies for the periodic patterns. The disagreements are prominent in D_{xx}/hu^* for the first bend and D_{yy}/hu^* for the cross-over part. These results indicate that the 2D S-RP is advantageous to estimate the dispersion coefficients by predicting the entire shape of the pollutant cloud compared to the 2D ST-RP.

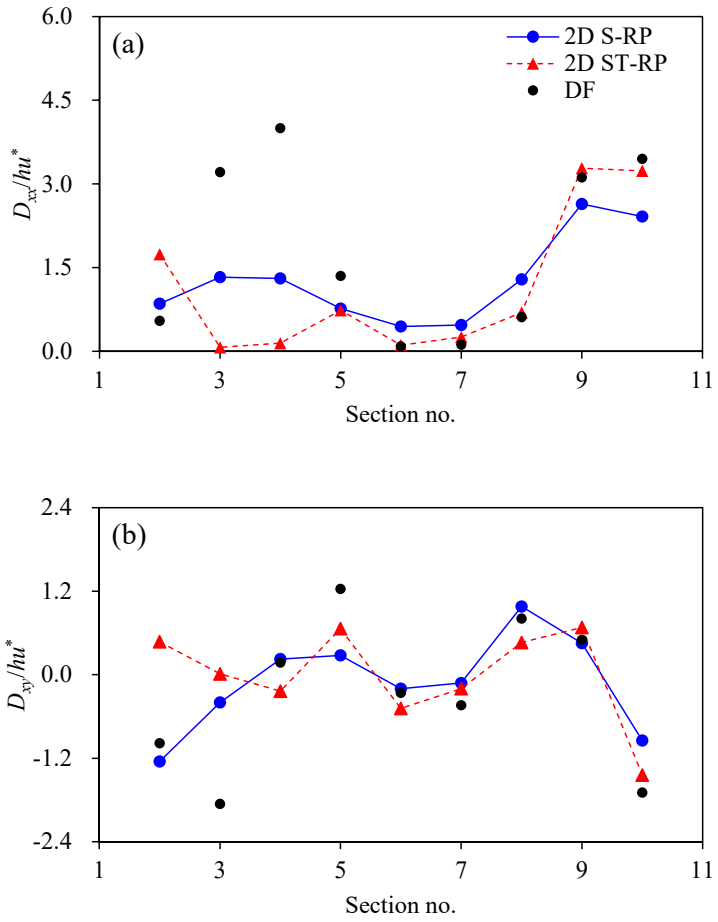

Figure 12. *Cont.*

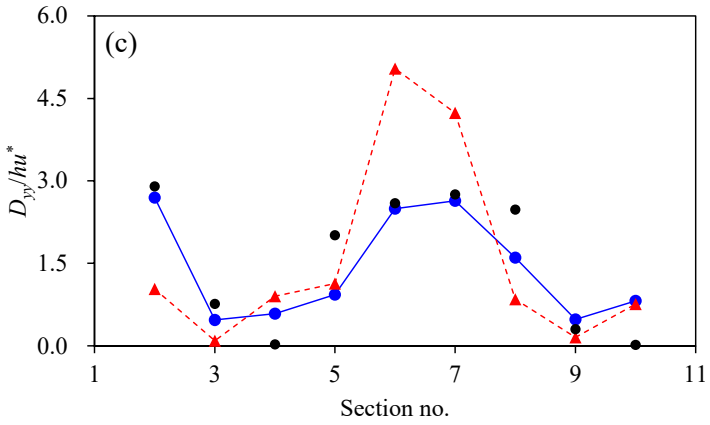

Figure 12. Comparisons of the spatial variabilities of the dispersion tensor: (**a**) D_{xx}/hu^*; (**b**) D_{xy}/hu^*; (**c**) D_{yy}/hu^*.

4. Discussions

4.1. Validity of the Frozen Cloud Assumption

The 2D ST-RP has been widely used to estimate the dispersion coefficients that originated from the temporal variations of concentration curves. However, due to the frozen cloud assumption, the 2D ST-RP is unsuitable for application in a mixing problem where the dispersion changes while a solute cloud crosses a measurement point. The limitations of the 2D ST-RP may lead to the inclusion of errors in estimated dispersion coefficients, whereas the 2D S-RP does not require incorporation of the assumption because the method uses the spatial distributions of concentration. Estimated dispersion coefficients using the 2D S-RP contain a history of the shear dispersion that occurred between the upstream and downstream concentration clouds. However, the 2D S-RP is limited in certain applications due to the difficulty in obtaining the spatial distribution of concentration.

To verify the validity of the frozen cloud assumption, the 2D ST-RP and 2D S-RP were applied for the ideal mixing problem. In the case of the 2D ST-RP, which requires a frozen cloud assumption, the concentration-time curve showed a relatively larger error in the continuously changing flow characteristics due to unsteady flow. The effectiveness of the frozen cloud assumption has been evaluated in previous studies [18,42,43]. Chatwin [42] mentioned that the frozen cloud assumption is not necessary when a pollutant cloud passes through a probe fast enough. In support of the explanation, Valentine and Wood [43] showed that the variance of the temporal concentration curve can be overestimated compared to the variance calculated from spatial data when the velocity of the pollutant cloud is slower than the actual flow velocity. Singh and Beck [18] also found errors in results of the routing procedure by skewed concentration curves and suggested a modified one-dimensional routing procedure. On the other hand, the 2D S-RP calculates the dispersion coefficient using the spatial concentration fields captured instantly, so if the non-Fickian mixing phenomenon due to the river topography did not appear, the dispersion coefficient could be calculated with very high accuracy.

Since the flow characteristics of most natural rivers are unsteady, the advection and dispersion of the polluted cloud due to the flow velocity change while the polluted cloud passes through a channel cross-section. Previous studies have suggested that the frozen cloud assumption is maintained, assuming that the flow remains constant while passing through the polluted cloud. However, as shown in the results of this study, it can be seen that in the region where the unsteady flow characteristics appear, the S-RP using the spatial distribution of concentration shows a more suitable result.

4.2. Applicability to Non-Fickian Mixing

The dispersion coefficients for the 2D tracer test conducted in the M2 channel were compared using the two routing procedures and the theoretical method using vertical

profiles of velocity. The 2D ST-RP used the concentration-time curves measured by the previous tracer study, and the 2D S-RP employed the spatial concentration distributions computed by the PDM-2D simulation results. The dispersion coefficients by the theoretical approach were considered as exact values because the additional dispersion due to channel irregularities can be neglected in the M2 channel. Each component of dispersion tensor showed periodic patterns along the channel, and the results by the 2D S-RP adequately reproduced the spatial variations of the dispersion in the meandering channel. These spatial variabilities in dispersion coefficients due to the growth and decay of secondary flows in the meander cycle have also been reported in a study by Boxall and Guymer [8,44]. However, the spatial changes by the 2D ST-RP showed discrepancies, which were deduced by the skewed concentration-time curves violating the frozen cloud assumption.

The non-Fickian mixing due to the storage zone of the river forms a long tail in the concentration-time curve, which causes difficulties with applying the mixing theory following the Fick's law. The storage zone causes an imbalance between vertical turbulent diffusion and shear advection and leads to asymmetric concentration curves [45]. This process was described in detail in the study by Denton [46]. When a pollutant cloud passes through a probe installed at a middle of water depth, concentration of the pollutant cloud located near the water surface is measured first due to fast flow velocity in the upper layer. After that, the probe measures concentration of the pollutant cloud near the channel bed, which goes to the upper layer by vertical mixing and relatively slow flow velocity. Therefore, it shows a difference from the shape of the polluted cloud observed at a specific time, and the frozen cloud assumption becomes invalid. The tracer test results of the M2 channel corresponds to the initial period that causes the imbalance of vertical diffusion and shear advection and shows a spatiotemporal asymmetric concentration distribution even though the storage zone is not included [30]. Since the 2D ST-RP and the 2D S-RP were derived from the Fickian dispersion model, both methods showed differences from the velocity-based dispersion tensor calculation results, as shown in Figure 12. However, even though the limitations originated from the Fick's law, the 2D S-RP is more advantageous for estimating the dispersion coefficient when the solute mixing shows non-Fickian characteristics.

5. Conclusions

In this study, two routing procedures using temporal concentration curves and spatial concentration distribution were evaluated against two solute mixing problems. Performance of the two routing methods was analyzed in two aspects: (1) validity of the frozen cloud assumption and (2) applicability to the non-Fickian solute mixing problem. The analysis results are summarized below.

- For a solute mixing problem under the unsteady flow condition, the 2D S-RP provides quite accurate estimation results of dispersion coefficients when the mixing shows the Fickian dispersion.
- The temporal concentration curves present the non-Fickian mixing due to the unsteady flow condition even though the solute cloud shows the Fickian dispersion. Thus, the dispersion coefficients by the 2D ST-RP using the temporal data contain errors due to violation of the frozen cloud assumption.
- Both the dispersion coefficients calculated by the 2D ST-RP and the 2D S-RP showed errors against to the results using the velocity-based method for the solute mixing in the initial period where the non-Fickian mixing occurs. These discrepancies showed that the two routing methods were derived based on the Fickian dispersion model.
- The results obtained using the 2D S-RP in the meandering channel more accurately exhibited the spatial variability along the meander cycle of dispersion coefficients compared to the 2D ST-RP.

From the aforementioned analysis results, the 2D S-RP is able to provide more reasonable results of dispersion coefficients in both the Fickian and the non-Fickian mixing problems than the 2D ST-RP if spatial distributions of concentration are available. These

conclusions are limited to the laboratory-scale application results since verifications have not been conducted on the natural river scale which has more complicated mixing properties. In future studies after the concentration measurement technique through the image analysis technique currently being studied has been established, it is expected that the applicability of the 2D S-RP can be evaluated on the field scale.

Author Contributions: Conceptualization, D.R. and I.P.; funding acquisition, D.R.; methodology, I.P.; project administration, D.R.; software, J.S.; validation, I.P.; visualization, J.S.; writing—original draft, J.S. and I.P.; writing—review & editing, J.S. and I.P. All authors have read and agreed to the published version of the manuscript.

Funding: This work is funded by the Ministry of Land, Infrastructure and Transport.

Institutional Review Board Statement: Not applicable.

Informed Consent Statement: Not applicable.

Data Availability Statement: The data presented in this study will be shared by the authors if requested.

Acknowledgments: This work is supported by the Korea Agency for Infrastructure Technology Advancement (KAIA) grant funded by the Ministry of Land, Infrastructure and Transport (Grant 21DPIW-C153746-03).

Conflicts of Interest: The authors declare no conflict of interest.

References

1. Fischer, H.B.; List, J.E.; Koh, R.C.Y.; Imberger, J.; Brooks, N.H. *Mixing in Inland and Coastal Waters*, 2nd ed.; Academic Press: San Diego, CA, USA, 1979; pp. 80–147.
2. Shen, C.; Niu, J.; Anderson, E.J.; Phanikumar, M.S. Estimating longitudinal dispersion in rivers using Acoustic Doppler Current Profilers. *Adv. Water Resour.* **2010**, *33*, 615–623. [CrossRef]
3. Kim, D. Assessment of longitudinal dispersion coefficients using Acoustic Doppler Current Profilers in large river. *J. Hydro-Environ. Res.* **2012**, *6*, 29–39. [CrossRef]
4. Lee, M.E.; Seo, I.W. Spatially variable dispersion coefficients in meandering channels. *J. Hydraul. Eng.* **2013**, *139*, 141–153. [CrossRef]
5. Park, I.; Seo, I.W.; Shin, J.; Song, C.G. Experimental and numerical investigations of spatially-varying dispersion tensors based on vertical velocity profile and depth-averaged flow field. *Adv. Water Resour.* **2020**, *142*, 103606. [CrossRef]
6. Jung, S.H.; Seo, I.W.; Kim, Y.D.; Park, I. Feasibility of velocity-based method for transverse mixing coefficients in river mixing analysis. *J. Hydraul. Eng.* **2019**, *145*, 04019040. [CrossRef]
7. Shin, J.; Seo, I.W.; Baek, D. Longitudinal and transverse dispersion coefficients of 2D contaminant transport model for mixing analysis in open channels. *J. Hydrol.* **2020**, *583*, 124302. [CrossRef]
8. Boxall, J.B.; Guymer, I. Analysis and prediction of transverse mixing coefficients in natural channels. *J. Hydraul. Eng.* **2003**, *129*, 129–139. [CrossRef]
9. Seo, I.W.; Park, S.W. Effects of velocity structures on tracer mixing in a meandering channel. *J. Korean Soc. Civil Eng.* **2009**, *29*, 35–45. (In Korean)
10. Yotsukura, N.; Sayre, W.W. Transverse mixing in natural channels. *Water Resour. Res.* **1976**, *12*, 695–704. [CrossRef]
11. Holley, F.M.; Nerat, G. Field calibration of stream-tube dispersion model. *J. Hydraul. Eng.* **1983**, *109*, 1455–1470. [CrossRef]
12. Zhang, W.; Zhu, D.Z. Transverse mixing in an unregulated North River. *J. Hydraul. Eng.* **2011**, *137*, 1426–1440. [CrossRef]
13. Baek, K.O. Flowchart on choosing optimal method of observing transverse dispersion coefficient for solute transport in open channel flow. *Sustainability* **2018**, *10*, 1332. [CrossRef]
14. Sayre, W.W.; Chang, F.M. *A Laboratory Investigation of Open Channel Dispersion Processes for Dissolved, Suspended, and Floating Dispersants*; USGS Professional Papers No. 433-E; United States Government Printing Office: Washington, DC, USA, 1968; pp. 59–61.
15. Holley, E.R.; Siemons, J.; Abraham, G. Some aspects of analyzing transverse diffusion in rivers. *J. Hydraul. Res.* **1972**, *10*, 27–57. [CrossRef]
16. Beltaos, S. Transverse mixing tests in natural streams. *J. Hydraul. Div.* **1980**, *106*, 1607–1625. [CrossRef]
17. Baek, K.O.; Seo, I.W. Routing procedures for observed dispersion coefficients in two-dimensional river mixing. *Adv. Water Resour.* **2010**, *33*, 1551–1559. [CrossRef]
18. Fischer, H.B. Dispersion predictions in natural streams. *J. Sanit. Eng. Div.* **1968**, *94*, 927–944. [CrossRef]
19. Singh, S.K.; Beck, M.B. Dispersion coefficient of streams from tracer experiment data. *J. Hydraul. Eng.* **2003**, *129*, 539–546. [CrossRef]

20. Baek, D.; Seo, I.W.; Kim, J.S.; Nelson, J.M. UAV-based measurements of spatio-temporal concentrqation distributions of fluorescent tracers in open channel flows. *Adv. Water Resour.* **2019**, *127*, 76–88. [CrossRef]
21. Legleiter, C.J.; McDonald, R.R.; Nelson, J.M.; Kinzel, P.J.; Perroy, R.L.; Baek, D.; Seo, I.W. Remote sension of tracer dye concentrations to support dispersion studies in river channels. *J. Ecohydraul.* **2019**, *4*, 131–146. [CrossRef]
22. Legleiter, C.J.; Manley, P.V.; Erwin, S.O.; Bulliner, E.A. An experimental evaluation of the feasibility of inferring concentrations of a visible tracer dye from remotely sensed data in turbid rivers. *Sensors* **2020**, *12*, 57. [CrossRef]
23. Taylor, G.I. The dispersion of matter in turbulent flow through a pipe. *Proc. R. Soc. Lond. A: Math. Phys. Eng. Sci.* **1954**, *223*, 446–468.
24. Piasecki, M.; Katopodes, N.D. Identification of stream dispersion coefficients by adjoint sensitivity method. *J. Hydraul. Eng.* **1999**, *125*, 714–724. [CrossRef]
25. Lee, M.E.; Seo, I.W. Analysis of pollutant transport in the Han River with tidal current using a 2D finite element model. *J. Hydro-Environ. Res.* **2007**, *1*, 30–42. [CrossRef]
26. Lee, M.E.; Seo, I.W. 2D finite element pollutant transport model for accidental mass release in rivers. *KSCE J. Civil Eng.* **2010**, *14*, 77–86. [CrossRef]
27. Alavian, V. Dispersion tensor in rotating flows. *J. Hydraul. Eng.* **1986**, *112*, 771–777. [CrossRef]
28. Seo, I.W.; Choi, H.J.; Kim, Y.D.; Han, E.J. Analysis of two-dimensional mixing in natural streams based on transient tracer tests. *J. Hydraul. Eng.* **2016**, *142*, 04016020. [CrossRef]
29. Fischer, H.B. *Methods for Predicting Dispersion Coefficients in Natural Streams, with Applications to Lower Reaches of the Green and Duwamish Rivers Washington (No. 582-A)*; US Government Printing Office: Washington, DC, USA, 1968; pp. 6–13.
30. Baek, K.O.; Seo, I.W.; Jung, S.J. Evaluation of transverse dispersion coefficient in meandering channel from transient tracer tests. *J. Hydraul. Eng.* **2006**, *132*, 1021–1032. [CrossRef]
31. Seo, I.W.; Baek, K.O.; Jeon, T.M. Analysis of transverse mixing in natural streams under slug tests. *J. Hydraul. Res.* **2006**, *44*, 350–362. [CrossRef]
32. Park, I.; Seo, I.W. Modeling non-Fickian pollutant mixing in open channel flows using two-dimensional particle dispersion model. *Adv. Water Resour.* **2018**, *111*, 105–120. [CrossRef]
33. Rozovskii, I.L. *Flow of Water in Bends of Open Channels*; Academy of Science of Ukrainian SSR: Moscow, Russia, 1957.
34. Jackson, P.S. On the displacement height in the logarithmic velocity profile. *J. Fluid Mech.* **1981**, *111*, 15–25. [CrossRef]
35. Odgaard, A.J. Meander flow model. I: Development. *J. Hydraul. Eng.* **1986**, *112*, 1117–1136. [CrossRef]
36. Seo, I.W.; Song, C.G. Numerical Simulation of Laminar Flow past a Circular Cylinder with Slip Conditions. *Inter. J. Numer. Methods Fluids* **2012**, *68*, 1538–1560. [CrossRef]
37. Song, C.G.; Seo, I.W.; Kim, Y.D. Analysis of secondary current effect in the modeling of shallow flow in open channels. *Adv. Water Resour.* **2012**, *41*, 29–48. [CrossRef]
38. Seo, I.W.; Kim, Y.D.; Song, C.G. Validation of Depth-Averaged Flow Model Using Flat-Bottomed Benchmark Problems. *Sci. World J.* **2014**, *2014*, 197539. [CrossRef] [PubMed]
39. Seo, I.W.; Kim, Y.D.; Song, C.G. Analysis of Flow Characteristics around Islands due to Semi-Diurnal Currents in the Han River, Korea. *KSCE J. Civil Eng.* **2015**, *19*, 1905–1915. [CrossRef]
40. Elder, J.W. The dispersion of marked fluid in turbulent shear flow. *J. Fluid Mech.* **1959**, *5*, 544–560. [CrossRef]
41. Rutherford, J.C. *River Mixing*; John Wiley and Sons: London, UK, 1994; pp. 62–63.
42. Chatwin, P.C. On the interpretation of some longitudinal dispersion experiments. *J. Fluid Mech.* **1971**, *48*, 689–702. [CrossRef]
43. Valentine, E.M.; Wood, I.R. Longitudinal dispersion with dead zones. *J. Hydraul. Div.* **1977**, *103*, 975–990. [CrossRef]
44. Boxall, J.B.; Guymer, I. Longitudinal mixing in meandering channels: New experimental data set and verification of a predictive technique. *Water Resour.* **2007**, *11*, 341–354. [CrossRef]
45. Chatwin, P.C. Presentation of longitudinal dispersion data. *J. Hydraul. Div.* **1980**, *106*, 71–83. [CrossRef]
46. Denton, R.A. Analytical asymptotic solutions for longitudinal dispersion with dead zones. *J. Hydraul. Res.* **1990**, *28*, 309–329. [CrossRef]